Light Metals 2011 *Edited by: Stephen J. Lindsay*
TMS (The Minerals, Metals & Materials Society), 2011

EXPERMENTAL INVESTIGATION OF SINGLE BUBBLE CHARACTERISTICS IN A COLD MODEL OF A HALL-HÉROULT ELECTROLYTIC CELL

Subrat Das[1], Yos Morsi, Geoffrey Brooks, William Yang[2], John J.J. Chen[3]
[1]Subrat Das, Yos Morsi, Geoffrey Brooks; Swinburne University of Technology, FEIS, PB 218, Hawthorn, VIC 3122, Australia
[2]William Yang; CSIRO, Minerals, Box 312, Clayton, VIC 3169, Australia
[3]John J.J. Chen; 20 Symonds Street, Dept. of Chem. and Materials Engineering, Auckland 1142, New Zealand

Keywords: Bubble dynamics, Wall induced forces, Hall-Héroult process, High speed photography

Abstract

Understanding the characteristics of the bubbles generated within a Hall-Héroult electrolytic cells, can assist greatly in the optimization and the operation of the process. One of the significant factors that greatly influence the bubbles formation is the vertical walls formed by the anodes. In this paper we used a high speed camera to investigate the effect of vertical walls on the shape of a single bubble rising in two liquids of high and low viscosity namely glycerol and water respectively under various offsets of the vertical wall and gas injection rates. The images of the bubble rising were recorded at the speed of 5000 frames per second and subsequently processed using the classical image-processing algorithms incorporated with MATLAB. The data related to various parameters such as aspect ratio, equivalent diameter of the bubble and bubble distance from the vertical wall are presented and discussed for various flow rate regimes. The findings showed that the presence of a vertical wall on one side of the bubble has a significant effect on the bubble shape, orientations and the trajectory path. In addition, it was found that as the bubble moved away from the wall, the velocity of the fluid between the bubble and the wall increased relative to the surrounding fluid, which created an asymmetric flow field around the bubble. Still the aspect ratios of the bubbles were found to be a function of the rate of gas injection as well as wall offset.

Introduction

The rising of bubbles in a viscous liquid due to buoyancy is a common phenomenon in chemical and metallurgical processes. The influence on volume, shape and terminal velocity of bubbles upon the rheological properties of fluids (density, viscosity, surface tension etc.) are thought to be of key importance in designing many such multi-fluid systems. The interaction between bubble and the wall is complex due to the wall induced drag forces, bubble shape and related oscillations. Thus, an understanding of the interactions between bubbles and solid walls is important for many practical applications.

The rise of a bubble in a viscous liquid is accompanied by deformation of the bubble, resulting in spherical, ellipsoidal and in some cases toroidal shapes. Numerical simulations render possible the prediction of overall shape development of several techniques such as front tracking method [1], the volume of fluid method [2], the Lattice–Boltzman method [3] and the level set method [4] are available for solving problems with moving boundaries and are discussed in an excellent review article by Hua et. al. [5] and Chen et. al. [6]. Complications associated with the advection of the interfaces between two dissimilar fluids have largely limited numerical studies to simplified cases. The primary obstacle is the numerical diffusion which results in the sharpness of the advancing phase front being blurred due to the presence of highly discontinuous properties of the interface. Thus most of these analyses have been limited to single drops and bubbles with small density ratios in inviscid flow.

A number of experimental studies have addressed aspects regarding bubble shape and the velocity field around individual bubbles using particle image velocimetry (PIV) and high speed cameras [7-9]. Several techniques such as laser induced fluorescence (LIF) and infrared shadow technique (IST) have been used to enhance the camera and PIV output [10, 11]. Previous mathematical modelling studies have shown that when the distance of the bubble interface to the wall is more than twice as large as the bubble diameter, there is practically little effect of the wall boundary conditions on the simulation results[12, 13]. But if the walls are not symmetrical, i.e. if the bubbles are nearer to the wall of one side of the container then the shape is greatly influenced by the surrounding hydrodynamic field.

A spherical bubble rising near a vertical wall exhibits a creeping flow due to migration forces. A larger bubble, closer to a wall at one side, will be affected more due to the wall induced asymmetric flow and may undergo significant deformations. Details of these migration forces that stem from nonlinearities in advection momentum transport and interfacial deformability to break the symmetry are discussed by Magnaudet et al. [14]. Moreover, bubbles can fluctuate in response to oscillations in the pressure field [15] in the liquid. This pressure gradient will have a significant effect while the flow field behind the bubble is asymmetric.

In many situations, a bubble encounters a boundary wall during its transport process, and a hydrodynamic interaction occurs between the bubble and the wall. One example of such application is an aluminium electrolytic cell, where the bubbles nucleating from anode surface move along the vertical wall of anode inducing a strong circulatory motion. There have been several studies on bubble induced flow in Hall-Héroult cell [6,7], but most of these works have mainly addressed the bulk behavior of the flow rather than the bubble movement itself. In this paper, an attempt is made to analyse bubble behavior as it moves along the vertical side of the anode. The main objective of this study is to determine the influence of a solid wall on the shape and the trajectory of the bubbles travelling parallel to the vertical wall.

Experimental

Apparatus

Experiments were conducted in a 0.2 x 0.2 m Perspex square tank of height 0.15 m. The bubble train was generated using a 6 mm diameter orifice placed near the sidewall. A schematic representation of the experimental setup is shown in Fig. 1. A continuous air supply with a rotameter is attached to the orifice to

generate a chain of bubbles (bubble train) using different air injection rates ranging from 0.1 to 0.5 lpm. These flow rates (of air) are generally very high for bubble formation in water and very low in viscous media like glycerol. Initially, the sidewall distance was chosen to be twice the size of orifice diameter where the wall effects are negligible. Provisions were also made to decrease the sidewall distance from the bubble train.

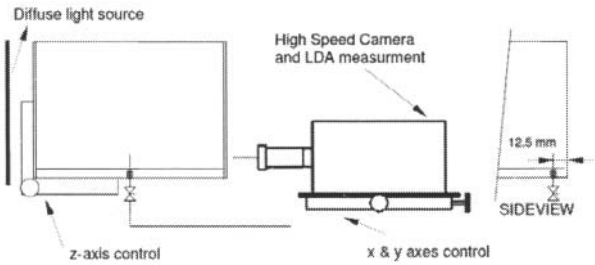

Figure 1. Experimental setup

Image Processing

The shape of bubble was studied using a high speed camera (FASTCAM-APX RS 250KC) at different wall offsets (WO). The camera was put on an automatic leveling shock-proof platform with precise x and y axes control. This enabled us to minimise the parallax error to a large extent. The continuous flow of bubbles was photographed at 5000 frames per second (fps) and images were processed using classical image-processing algorithms. The major source of uncertainty in the bubble diameter is the definition of the threshold in the setting of the digital image system. However, this error is a decreasing function of increasing bubble diameter. Bubble diameters in this study are fairly large (> 7 mm dia.) and thus the measurement of bubble dimensions are within reasonable accuracy.

The images from high speed camera are analysed binary and/or edge bubble images. Based on binary image-processing techniques, in which a binary image is defined by a characteristics function *b(x,y)* that takes on the values 0 or 1 and the area of the bubble or the binary image is:

$$A_b = \iint b(x,y)\,dxdy \qquad (1)$$

where this integration is over the whole image *I*.

The position of the centre of bubble in each frame can be obtained as follows:

$$\bar{x} = \frac{1}{A_b}\iint x b(x,y)\,dxdy = \frac{1}{A_b}\int x w(x,y)\,dx \qquad (2)$$

$$\bar{y} = \frac{1}{A_b}\iint y b(x,y)\,dxdy = \frac{1}{A_b}\int x h(x,y)\,dx \qquad (3)$$

Where *w(x,y)* and *h(x,y)* are the horizontal and vertical projections of the bubble on the x-axis and y-axis.

Matlab Image Processing toolbox is used to calculate area, centroid position, perimeter of the bubble in each time frame [16, 17]. The eccentricity and orientation are calculated by fitting an ellipse onto the circle. Their contours are extracted and measured by calibrating the image pixel length to millimeters.

Results and Discussions

As has been reported by many authors, the shape of the bubbles is very different with fluid property and the rate of injection. But in all non-Newtonian fluids, bubbles evolve from spherical shape to the teardrop shape when it detaches from the bottom surface [18, 19]. During this transition (from spherical to teardrop shape), bubbles exhibit different shapes as well as growth rate[20] depending upon the properties of the surrounding fluid. In the present work, five different flow rates of air (0.1 lpm to 0.5 lpm) are considered to create a chain of bubbles (bubble train) near a solid wall. At such injection rates of air, the deformation of the bubble and the flow pattern of the surrounding fluid would be completely different due to the viscosity of the fluid. In the case of water, the bubble deformations are accompanied with wobbling and oscillation exhibiting typical shape characteristics of the high Reynolds numbers regime. In the highly viscous situation like glycerol, the deformations are negligible at the initial growth period as the flow is in the low Reynolds number regime. In the following table the properties of glycerol and water are given:

Table 1. Fluid Properties

Fluids	Density ($kg.m^{-3}$)	Viscosity		Surface Tension σ ($mN.m^{-1}$)
		(Pa s)	ν (m^2/s)	
Glycerol (99%)	1260	1.2	9.5e-4	62
Water	1000	1e-3	1e-6	72
Electrolyte for H-H cell	2100	2.5e-3	1.2e-6	136.0

Analysis of shape of the bubble

Figure 2 shows the teardrop shape of a detached bubble at sidewall distance of 12.5 and 6.5 mm for the experiment using glycerol. The symmetry-axis remains along the direction of bubble motion at WO of 12.5 mm showing negligible interaction. Bubble tends to incline towards the solid wall, as side channel width (wall offset) reduces showing the departure of symmetrical shape, which may be attributed to the pressure gradient causing fluid to move towards the base of the bubble from the wall. In glycerol, the onset of departure from the symmetric line is observed even before the detachment of bubble (Figure 2b). At a wall offset of 6.5 mm, the mass flow between the wall and bubble prevents the bubble from contacting the wall. The bubble elongates due to the shear force that it generated in the gap which is an important observation of this study.

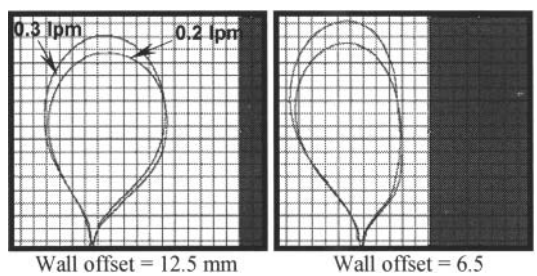

Figure 2. Bubble shape in glycerol at the time of detachment

The reference frame is one when the bubble is just detached from the base of the tank (t_{ref} = 0) which is shown in all the figures given below. In figure 3, the bubble trajectory is plotted sequentially at different sidewall offset for water and glycerol media respectively. Bubble contours are plotted at 40 frames apart, i.e. at 8 ms time interval. In glycerol, the bubbles move upward steadily as shown in Fig. 3a without any wobbling giving rise to a trajectory of rectilinear path[21].

The velocity of the fluid in the gap (between wall and bubble interface) increases with decreasing side channel width. The imbalance between the velocity of the fluid in the gap and the surrounding fluid gives rise to an asymmetric flow pattern at the trailing edge of the bubble. At a wall offset of 6.5 mm (Fig 3a-III) the bubble not only changes it shape and orientation but also elongates significantly due to the shear force arising from the high velocity within the gap. The initial deformation of bubble in both water and glycerol is observed due to the induced wall migration forces indicating dominating effect of the wall in general. The bubble is subjected to both rotational and translational displacement due to the presences of asymmetric forces caused due to the presence of a solid wall in the near vicinity. In the case of the less viscous fluid, water, shape deformation and oscillation becomes a dominating mode due to the pressure gradient in the surrounding fluid. In this case, bubbles rise upward in a jig-jag trajectory pattern. The general features of the rise of a gas bubble in a liquid, and its distortion at a high Bond number and Reynolds number are discussed elsewhere [6].

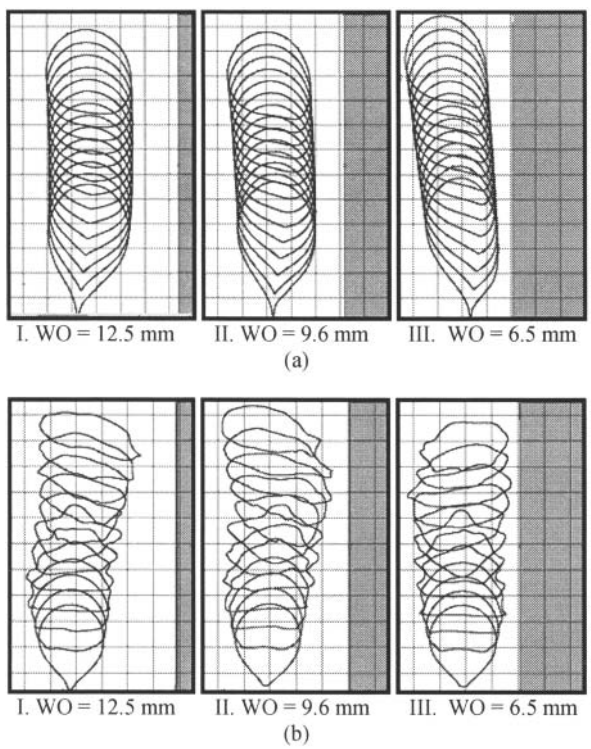

Figure 3. Bubble contours at 8ms interval of time in (a) Glycerol and (b) water respectively at 0.2 lpm

When the bubble begins to rise owing to buoyancy, the pressure gradient at the lower surface of the bubble is higher than that at the top surface, which deforms the lower surface significantly. The contour plots in figure 3 clearly show that the distance between successively images decreases with time indicating an initial deceleration. The initial, higher velocity created by air injection is affected by the viscosity of the fluid.

Figure 4 and 5 shows the contours of bubbles at a lesser time interval for the case of water to bring out the finer changes in shape and orientation due to the presence of the solid wall. Each row of the figure 4 and 5 shows the first 15 frames at 2 ms interval right after the detachment for WO of 12.5 and 6.5 mm respectively.

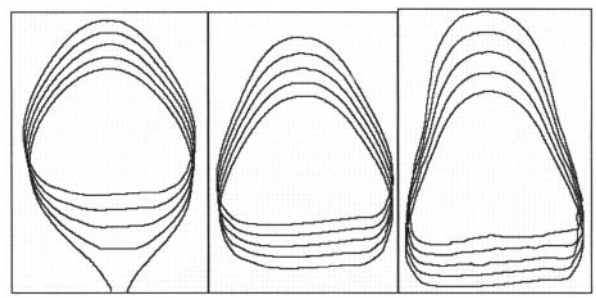

Figure 4. First fifteen consecutive frames at 2 ms apart for WO of 12.5 mm and 0.5 lpm gas injection rate in water.

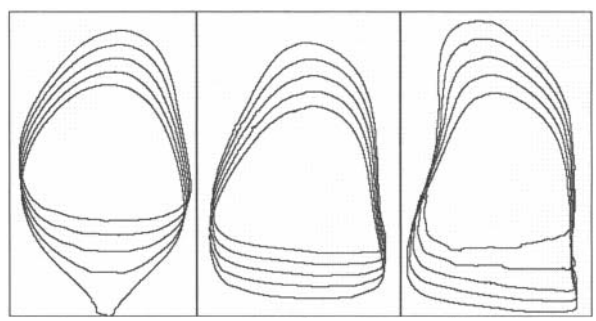

Figure 5. First fifteen consecutive frames at 2 ms apart for WO of 6.5 mm and 0.5 lpm gas injection rate in water.

The initial contours (first 5 frames) are quite symmetrical when the wall offset is twice the size of the bubble diameter in all sizes of bubbles. The bubble loses this symmetric nature as it rises further along the plume. It is to be noted that the change in shape of bubble, no matter how small it is, may initiate a lift force along with other migration forces. In the case of larger bubble the asymmetric shape is more apparent; this may be due to the higher bubble induced flow. When the bubble is closer to a wall the mass flow in the gap is much higher than in the surrounding. The tip tends to elongate as shown in the figure. This downward flow (in the gap) does not continue further going downward it rather tends to follow the bubble as a negative pressure field is created behind the bubble by the bubble deformation itself.

The aspect ratio (AR) and other parameters of the image are calculated using following equations.

$$AR = \frac{h}{w} \tag{4}$$

The rise velocity (v) is calculated from the mass centre (x and y coordinates) of the bubble over two consecutive frames (i, i+1) as:

$$v = \frac{\sqrt{(\bar{x}_{i+1} - \bar{x}_i)^2 + (\bar{y}_{i+1} - \bar{y}_i)^2}}{\Delta t} \tag{5}$$

It is to be noted that in 5000 frames per second data acquisitions, Δt is equivalent to 0.0002 s.

The maximum and minimum diameter were determined by the best-fitted ellipse to the 2d-bubble image [22] and compared with image dimension as well (Fig. 6). In figure 6, the pixel of the image is calibrated with mm scale and w and h refer to major and minor axes of the bubble.

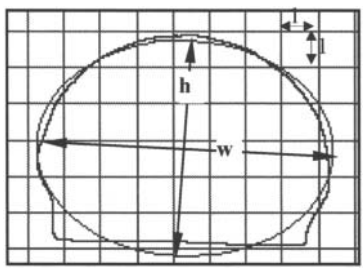

Figure 6. The bubble (at t = 14ms) and the best fitted ellipse

The equivalent diameter (d_e) and volume are calculated assuming axial symmetry [22, 23] over the direction of bubble trajectory:

$$d_e = (hw^2)^{1/3} \tag{6}$$

$$V_e = \frac{d_e^3 \pi}{6} \tag{7}$$

The bubbles have a visible indentation or a dimple at the base right after the detachment causing a shape transformation from spherical to asymmetric toroidal shapes within a small span of time. The shape change is obviously a manifestation of toroidal wake accompanying the bubble. This is the characteristic of bubble shapes at high Reynolds number flow. Thus, it becomes difficult to predict the volume from the 2-D projected images using equ. 7. However, the projected area of the image may be a better representation of the bubble shape during initial growth. Figure 7 represents the projected area vs. time in glycerol showing significant changes in shape with the decrease in wall offset.

Figure 8 plots the variation of aspect ratio with time for the bubble in glycerol and found to be in good agreement with previously published data [13, 24]. The aspect ratio are calculated (equ. 4 and Fig. 6) for the bubble in each time frame starting from the reference frame. A high aspect ratio at initial position ($t_{ref} = 0$) in figure (Fig. 8) indicates a teardrop shape of bubble in glycerol [18]. The rate of change of aspect ratio with time is very slow due to the viscosity of the glycerol. The influence of presence of the sidewall in the vicinity can be realised as the bubble evolve from bottom of the tank (t_{ref}=0, Fig.2b and Fig. 5). And also, in figure 8 the percentage change in aspect ratio is nearly 10% due to the sidewall. The aspect ratio (AR) of the bubble is always higher at lower channel width indicating significant elongation bubble tip (Fig. 5). The bubble tip elongates due to the shear force that generated between the wall and bubble.

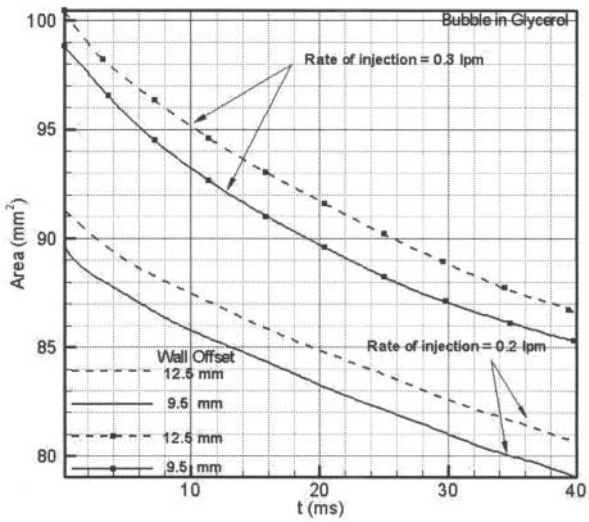

Figure 7. Projected Area vs. Time

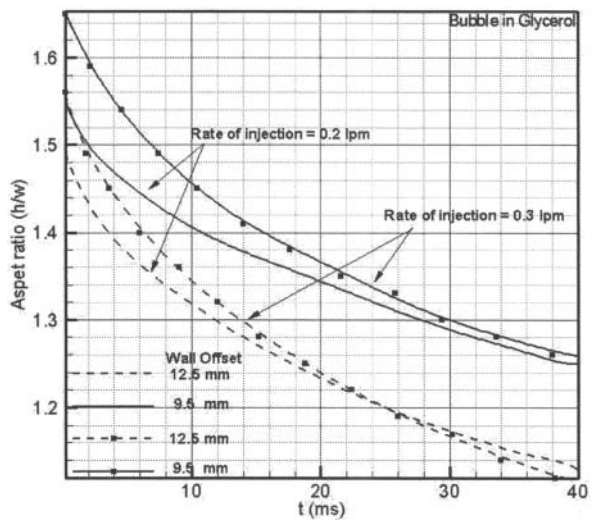

Figure 8. Aspect ratio vs. Time for bubble in glycerol

Bubbles in a water column with similar flow rates behave differently (Fig. 9). The bubble changes its teardrop shape (prolate) to spherical shape, within 3 ms of time after the detachment, and then to ellipsoidal and toroidal capped bubbles (oblate) as it rises further [19]. The width of the bubble changes

significantly when compared with glycerol. This can be attributed to the lower viscosity of water.

If one compares the results in terms of aspect ratio between glycerol (Fig. 8) and water (Fig. 9), it can be seen that the influence of sidewall on the geometric properties and velocity of the bubble can be measured at higher viscosity fluid but very much unpredictable in a lower viscosity fluid like water. The unpredictable influence of the sidewall in water is mainly attributed to the oscillation in the bubble-fluid interface. But the influence of sidewall cannot be ignored. The wall migration force changes the shape of bubble which is the main cause of wall induced lift force. This, in turn gives rise to a bubble trajectory path and bubble induced flow in the surrounding fluid. This phenomenon has a direct implication in Hall-Héroult cell where the bubbles near the vertical side of carbon anode would experience similar forces and can contribute significantly to the circulation flow patterns that occur in the side channel of the electrolytic cell. With reference to Table 1, the kinematic viscosities of water and the electrolyte of the Hall-Héroult cell are of similar magnitude. Thus if Reynolds Number is the major influencing factor, the results found for water may be assumed to be applicable. Further experimental and modeling work is required to fully quantify these effects.

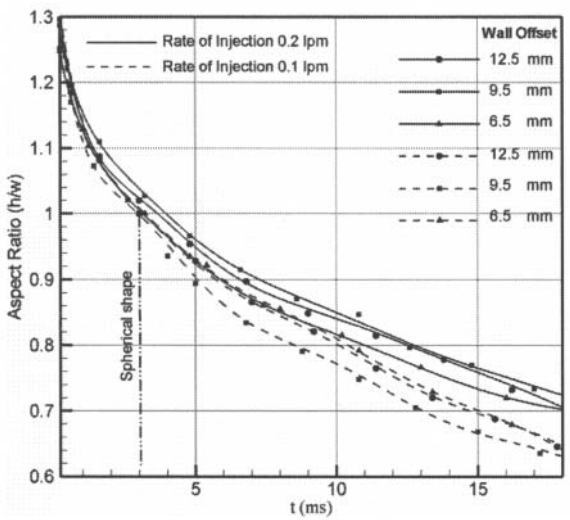

Figure 9. Aspect ratio vs. Time for bubble in water

Conclusion

The effect of sidewall on the shape of the bubble was studied experimentally in both water and glycerol. Different flow rates of air were used from the bottom of the tank to generate chains of bubbles. In general the results indicated that the bubbles lost their symmetric shape right after the detachment when sidewall was at a close proximity. The bubble also showed tendency to elongate as the side channel width decreased.

The data presented in this paper by our visualization technique and image processing was sufficiently accurate to allow us to predict not only the velocity but also the shape as well the orientation of the bubble. In future we are planning to analyze the complete hydrodynamic field including wall induced lift force that produced due to the bubble departure from symmetric shape to asymmetric one. Furthermore, the predicted data of various operating conditions will be validated using Particle Image Velocimetry (PIV).

Acknowledgements

This work was supported by the Breakthrough Technologies for Primary Aluminium Research Cluster - a collaborative research effort between CSIRO Light Metals Flagship, Swinburne University of Technology, University of Auckland, University of New South Wales, University of Wollongong and the University of Queensland, focused on developing technology to lower the overall energy consumption associated with primary aluminium production.

References

1. S. O. Unverdi, "A front-tracking method for viscous, incompressible, multifluid flows," *Journal of Computational Physics*, 100(1) (1992), 25-37.
2. W.J. Rider, and D.B. Kothe, "Reconstructing Volume Tracking," *Journal of Computational Physics*, 141(2) (1998), 112-152.
3. N. Takada, et al., "Numerical simulation of two- and three-dimensional two-phase fluid motion by lattice Boltzmann method", *Computer Physics Communications*, 129(1) (2000), 233-246.
4. S. Osher, and R.P. Fedkiw, "Level Set Methods: An Overview and Some Recent Results," *Journal of Computational Physics*, 169(2) (2001), 463-502.
5. J. Hua, J.F. Stene, and P. Lin, 'Numerical simulation of 3D bubbles rising in viscous liquids using a front tracking metho," *Journal of Computational Physics*, 227(6) (2008), 3358-3382.
6. L. Chen, et al., "The development of a bubble rising in a viscous liquid," *Journal of Fluid Mechanics*, 387 (1999), 61-96.
7. W. Yang, and M.A. Cooksey, "Effect of slot height and width on liquid flow in physical models of aluminium reduction cells," *TMS Light Metals*, (2007), 451-456.
8. K. Sakakibara, et al., "Measurement of the surrounding liquid motion of a single rising bubble using a Dual-Camera PIV system," *Flow Measurement and Instrumentation*, 18(5) (2007), 211-215.
9. Z, Liu, and Y. Zheng, "PIV study of bubble rising behavior," *Powder Technology*, 168(1) (2006), 10-20.
10. A. Tokuhiro, et al., "Turbulent flow past a bubble and an ellipsoid using shadow-image and PIV techniques," *International Journal of Multiphase Flow*, 24(8) (1998), 1383-1406.
11. A. Fujiwara, D. Minato, and K. Hishida, "Effect of bubble diameter on modification of turbulence in an upward pipe flow," *International Journal of Heat and Fluid Flow*, 25(3) (2004), 481-488.
12. I. Chakraborty, I., et al., "Computational investigation on bubble detachment from submerged orifice in quiescent liquid under normal and reduced gravity," *Physics of Fluids*, 21(6) (2009)
13. C. Chen, and L.S. Fan, "Discrete Simulation of Gas-Liquid Bubble Columns and Gas-Liquid-Solid Fluidized Bed," *AIChE Journal*, 50(2) 2004, 288-301.
14. J. Magnaudet, S. Takagi, and D. Legendre, "Drag, deformation and lateral migration of a buoyant drop moving near a wall," *Journal of Fluid Mechanics*, 476 (2003), 115-157.

15. K, Lunde, and R. J. Perkins, "Shape oscillations of rising bubbles," *Applied Scientific Research*, 58(1-4) (1997), 387-408.
16. C. Beggan, and C.W. Hamilton, "New image processing software for analyzing object size-frequency distributions, geometry, orientation, and spatial distribution," *Computers & Geosciences*, 36(4) (2010), 539-549.
17. C. Igathinathane, et al., "Shape identification and particles size distribution from basic shape parameters using ImageJ," *Computers and Electronics in Agriculture*, 63(2) (2008), 168-182.
18. D. Funfschilling, and H.Z. Li, "Effects of the Injection Period on the Rise Velocity and Shape of a Bubble in a Non-Newtonian Fluid," *Chemical Engineering Research and Design,* 84(10) (2006), 875-883.
19. W. Fan, et al., "Study on bubble formation in non-Newtonian fluids by laser image technique", *Optics & Laser Technology*,40(2) (2008), 389-393.
20. A. Vazquez, et al., "A look at three measurement techniques for bubble size determination," *Experimental Thermal and Fluid Science*, 30(1) 2005, 49-57.
21. G. Brenn, V. Kolobaric, and F. Durst, "Shape oscillations and path transition of bubbles rising in a model bubble column," *Chemical Engineering Science*, 61(12), 2006, 3795-3805.
22. W. Kracht, and J.A. Finch, "Effect of frother on initial bubble shape and velocity," *International Journal of Mineral Processing*, 94(3-4) (2010), 115-120.
23. Y. Saito, et al., "Shape measurement of bubble in a liquid metal," *Nuclear Instruments and Methods in Physics Research Section A: Accelerators, Spectrometers, Detectors and Associated Equipment*, 605(1-2) (2009), 192-196.
24. R. Clift, J. R. Grace, and M. E. Weber, "Bubbles, drops and Particles,". 1978.